International Journal of Plasticity 37 (2012) 108–118

Contents lists available at SciVerse ScienceDirect

International Journal of Plasticity

journal homepage: www.elsevier.com/locate/ijplas

Increased time-dependent room temperature plasticity in metallic glass nanopillars and its size-dependency

Byung-Gil Yoo [a], Ju-Young Kim [b], Yong-Jae Kim [a], In-Chul Choi [a], Sanghoon Shim [c], Ting Y. Tsui [d], Hongbin Bei [e], Upadrasta Ramamurty [f], Jae-il Jang [a,*]

[a] Division of Materials Science and Engineering, Hanyang University, Seoul 133-791, Republic of Korea
[b] School of Mechanical and Advanced Materials Engineering, UNIST, Ulsan 689-805, Republic of Korea
[c] Architecture and Offshore Research Department, Research Institute of Industrial Science and Technology, Inchon 406-840, Republic of Korea
[d] Waterloo Institute of Nanotechnology, University of Waterloo, Waterloo, ON, Canada N2L 3Gl, Canada
[e] Materials Science and Technology Division, Oak Ridge National Laboratory, Oak Ridge, TN 37831-6115, USA
[f] Department of Materials Engineering, Indian Institute of Science, Bangalore 560012, India

ARTICLE INFO

Article history:
Received 1 December 2011
Received in final revised form 23 April 2012
Available online 11 May 2012

Keywords:
Metallic glass
Time-dependent plasticity
Nanomechanical properties
Size effect
Nanopillar

ABSTRACT

Room temperature, uniaxial compression creep experiments were performed on micro-/nano-sized pillars (having diameters in the range of 250–2000 nm) of a Zr-based bulk metallic glass (BMG) to investigate the influence of sample size on the time-dependent plastic deformation behavior in amorphous alloys. Experimental results reveal that plastic deformation indeed occurs at ambient temperature and at stresses that are well below the nominal quasi-static yield stress. At a given stress, higher total strains accrue in the smaller specimens. In all cases, plastic deformation was found to be devoid of shear bands, i.e., it occurs in homogeneous manner. The stress exponent obtained from the slope of the linear relation between strain rate and applied stress also shows a strong size effect, which is rationalized in terms of the amount of free volume created during deformation and the surface-to-volume ratio of the pillar.

1. Introduction

The physics of plastic deformation in metallic glasses is distinctly different from their crystalline counterparts due to the absence of long-range periodicity and hence dislocations. While dislocation activity is the main reason for accrual of plastic strains upon loading of crystalline materials, plastic deformation in metallic glasses occurs through shear transformation zones (STZs, that are the fundamental carriers of plasticity) and then shear bands, and its plasticity is intrinsically controlled by the 'free volume' in it. With the recent discovery of bulk metallic glasses (BMGs) offering high strength and moderate toughness, considerable interest is evinced by the research community in understanding plasticity of metallic glasses. One of the distinct features of the mechanical behavior of BMGs is the temperature- and stress-dependent deformation mode in BMGs (Argon, 1979; Schuh et al., 2007; Spaepen, 1977). At high temperatures (above the glass transition temperature T_g) and low stresses, STZs operate profusely and hence the flow is homogeneous. In contrast, localized plastic flow, in terms of shear bands, dominates at relatively low temperatures and sufficiently high stresses. By far, this feature has led to considerable activity in trying to understand the origins and kinetics of shear bands and their relationship with ductility and toughness. Recently, some simulations and experiments demonstrated that at sufficiently long loading periods, homogeneous deformation can be observed even when the applied stresses are well below the nominal yield strength, σ_y, at room temper-

* Corresponding author.
E-mail address: jijang@hanyang.ac.kr (J.-i. Jang).

0749-6419/$ - see front matter © 2012 Elsevier Ltd. All rights reserved.
http://dx.doi.org/10.1016/j.ijplas.2012.04.005

ature (RT) (Albano and Falk, 2005; Falk and Langer, 1998; Lee et al., 2008; Park et al., 2008, 2009a,b). While atomistic simulations have suggested that such loads can produce irreversible changes in the glass structure (Albano and Falk, 2005; Falk and Langer, 1998), creep-like behavior at RT was experimentally observed through the uniaxial elastostatic compression tests in mm-sized Cu–Zr (Lee et al., 2008; Park et al., 2008, 2009a,b) and Zr-based (Ke et al., 2011) BMG samples.

One of the highly active research areas, in the context of mechanical behavior of materials, has been the size effects on mechanical properties such as strength and ductility. For crystalline materials, it has been well documented that the size of sample, and the length scale of the microstructural unit (such as the grain size), and the size of the deforming zone may significantly affect the mechanical behavior (Kim et al., 2011; Greer and De Hosson, 2011). The 'size-dependence' of the properties in metallic glasses (where no crystalline defects can be defined) has also evinced interest as there is sufficient technological interest in using them for micro-/nano-components in micro-electro-mechanical system (MEMS) such as gears, mirrors and membranes (Chen, 2011; Inoue and Takeuchi, 2011; Kumar et al., 2011; Schroers, 2010; Wang, 2009). While it has been reported that the deforming volume size (e.g., indentation size effect) may also follow the 'smaller, stronger' concept in metallic glasses (Jang et al., 2011b; Van Steenberge et al., 2007), the sample size effect observed from uniaxial micro-/nano-pillar tests is somewhat controversial; some researchers showed 'smaller is stronger (Jang and Greer, 2010; Jang et al., 2011a; Schuster et al., 2008; Shan et al., 2008; Ye et al., 2009),' whereas others reported the opposite softening trend (Huang et al., 2007; Volkert et al., 2008). It has been also proposed that the strength of BMG is actually size-independent (Chen et al., 2010; Dubach et al., 2009).

Our attention has been drawn to the fact that the size effect on time-dependent plastic deformation of metallic glasses has never been analyzed through uniaxial micro-/nano-pillar creep experiments, despite the importance of understanding such deformation at small scale in the materials' applications to micro-/nano-scale components. The work reported in this paper is conducted in this spirit, with the particular objective of examining whether the creep-like response in metallic glass exhibits size-dependent or not? A number of nanoindentation creep studies have been performed on metallic glasses (Castellero et al., 2008; Huang et al., 2009a,b; Li et al., 2008; Yoo et al., 2010a,b). However, the stress state underneath the indenter is complex and hence deductions on the operative physical mechanisms are not straightforward (Wang et al., 2010). Keeping this in view, for the first time, we have performed RT creep experiments in uniaxial compression on different sized micro- and nano-pillars of a Zr-based metallic glass, which are reported in this paper.

2. Experiments

The material examined in this work is a Zr-based BMG, $Zr_{52.5}Cu_{17.9}Ni_{14.6}Al_{10}Ti_5$ (commercially designation: Vit 105), which was produced in the form of a rod having diameter and length of about 7 and 70 mm respectively. The amorphous nature of the sample was confirmed by the absence of crystalline peak in X-ray diffraction pattern (shown elsewhere (Yoo et al., 2009b)). After cutting the rod samples into ~1 mm disk-shaped specimens, the surfaces were ground with SiC papers, and then polished with a cloth using 0.3 μm alumina.

Pillars having various diameters (~250, 500, 1000, and 2000 nm) were fabricated through the focused ion beam (FIB) milling with a Nova 200 NanoLab (FEI Co., Hillsboro, OR, USA) following the method described in Ref. (Kim and Greer, 2009). More than 20 pillars for each diameter were fabricated by top–down ion beam patterning with the final ion current of 0.1 nA and at a constant ion accelerating voltage of 30 kV. The pillars were made to reside at the center of a 50 μm crater, which provides enough space for the indenter to come down on the sample during the test without contacting the crater rim.

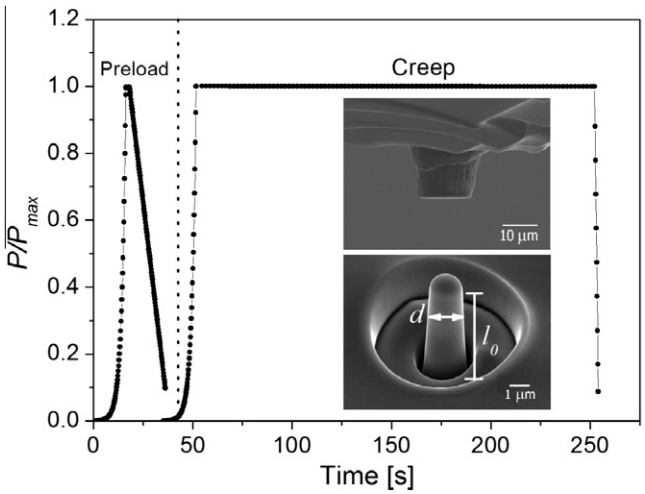

Fig. 1. Schematic illustration of the creep testing sequences. Inset micrographs show 17 μm-diameter flat punch tip and a 2000 nm-diameter pillar.

The aspect ratio in all pillars was maintained at ~3 so that the relative contributions from friction and constraint at the ends of pillars remain constant (Chen et al., 2010; Dubach et al., 2009; Schuster et al., 2008; Shan et al., 2008; Volkert et al., 2008; Ye et al., 2009).

Time-dependent deformation experiments were performed using the Nanoindenter-XP (Agilent Corp., Oak Ridge, TN, USA) with a FIB-milled cylindrical diamond punch whose top diameter is ~17 μm (see the inset of Fig. 1). A major issue while conducting creep experiments with a nanoindenter is the thermal drift. To avoid any possible experimental artifacts associated with it, thermal drift was maintained below 0.05 nm/s. Fig. 1 shows a schematic illustration of the testing procedure adapted. Prior to the creep segment, a preload was applied (with the same stress as that applied during the subsequent creep test) so to minimize the top surface effects (Chen et al., 2010; Dubach et al., 2009; Jang et al., 2011a; Volkert et al., 2008). During the creep test, the load was increased up to the desired maximum stress level (i.e., 400, 600, 800,

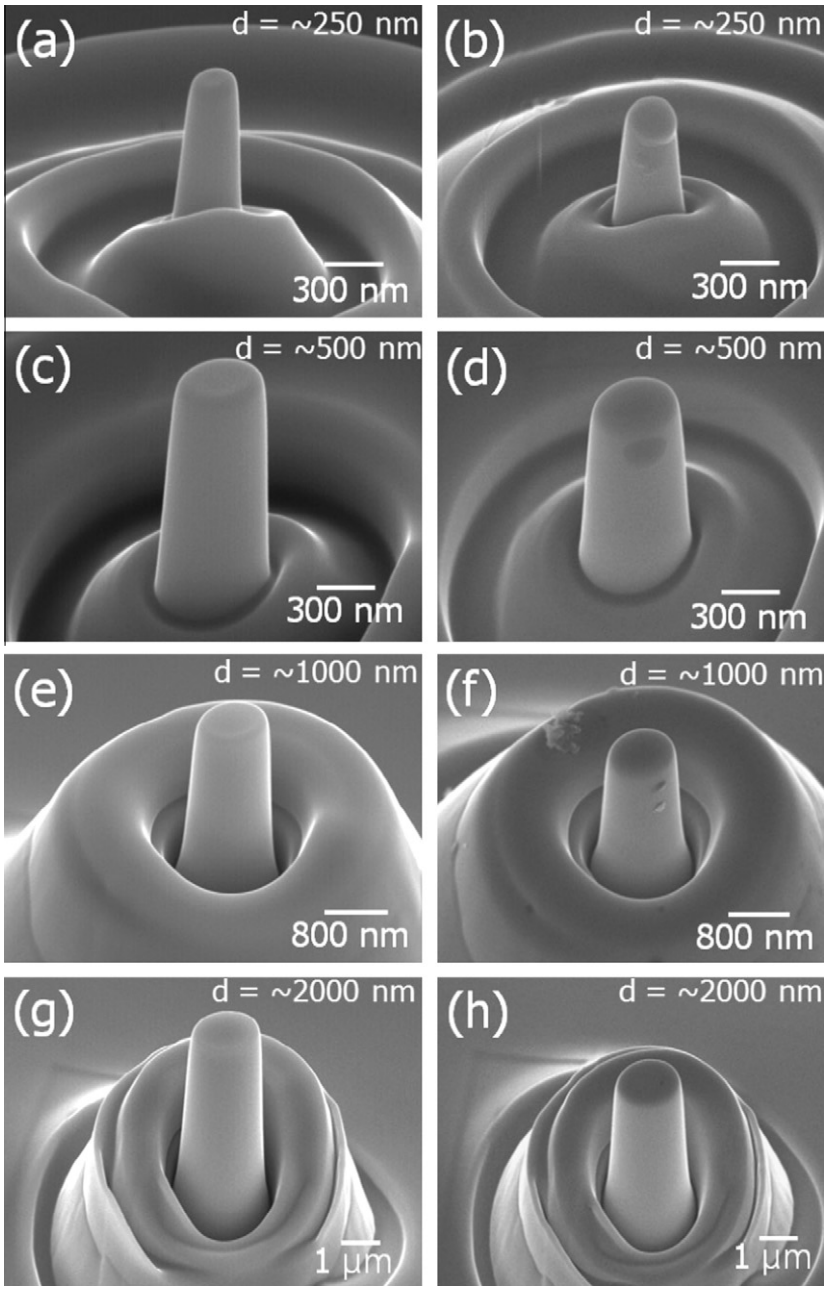

Fig. 2. Representative SEM images of pillar before [(a), (c), (e), (g)] and after [(b), (d), (f), (h)] the creep test (at σ = 1000 MPa); (a), (b) for 250 nm, (c), (d) for 500 nm, (e), (f) for 1000 nm, and (g), (h) for 2000 nm, respectively.

1000 MPa, respectively) at a fixed loading rate, $(dP/dt)/P = 1/s$, then held for 200 s, and finally removed at the same rate as the loading segment. The holding time was chosen in consideration of the thermal and the instrumental drift (Yoo et al., 2010a). From the recorded indentation load–displacement (P–h) data, the engineering stress σ and engineering strain ε were calculated as $\sigma \sim P/[\pi(d/2)^2]$ and $\varepsilon \sim h/l_0$, respectively, where d is the pillar diameter (empirically determined as the diameter measured at ~30% of the pillar height from the pillar top for considering tapering effect) and l_0 is the initial height of pillar (see the inset of Fig. 1). Morphology of each pillar was imaged before and after creep test using scanning electron microscopy (SEM), JSM-6330F (JEOL Ltd., Tokyo, Japan).

3. Results

3.1. Deformation morphology

Fig. 2 shows a series of scanning electron microscopy (SEM) images of the pillars taken before and after the creep experiments conducted at a stress of 1000 MPa, the highest stress level at which creep experiments were conducted in this study. In all cases, no shear bands could be observed in any of the pillars. In addition, the displacement-time plots did not exhibit any prominent serrations or strain-bursts, which are usually associated with the inhomogeneous flow through shear band nucleation and propagation. This indicates that the creep deformation that is explored in this work is essentially homogenous in nature for all sample sizes. Unlike pillars having a larger diameter, the ~250 nm diameter pillar that was crept exhibits relatively larger deformation near the top than in the rest of the pillar. This difference may be related with the difficulties in controlling precise pillar shape (especially at smaller pillar diameters) and thus relatively severe top roundness and non-planarity in such a small pillar (Volkert et al., 2008; Zhang et al., 2006).

3.2. Engineering stress vs. strain

In Fig. 3, representative plots (for d = ~500 nm) of the engineering stress vs. engineering strain obtained from creep tests are shown along with those obtained in quasi-static compression of the same-sized pillar. Overlapping of the loading portion of the creep test curves with that of the quasi-static test indicates that the stress applied at the onset of creep is within the nominal elastic regime for this BMG. The most important feature in the figure is that the creep indeed occurs well below the nominal yield strength of 1.78 GPa for this BMG (measured through uniaxial compression experiments on macroscopic samples having a diameter of 7 mm (Bei et al., 2010)). It is also noteworthy in the figure that the amount of creep strain, ε, is found to increase significantly with σ. This stress-dependency of the creep strain indicates that the observed creep behavior is not an artifact caused by thermal drift which does not depend on load (and thus stress).

3.3. Creep strain

Fig. 4 provides representative ε vs. hold time, t, plots. The influences of σ, and the pillar diameter, d, on the creep strain are highlighted in this figure; i.e., ε increases with increasing σ and decreasing d. The ε–t curves are smooth (without any prominent serrations or pop-ins indicating inhomogeneous deformation) and mostly parabolic in nature (especially for higher σ and smaller d). This behavior is similar to those reported for high-temperature creep of crystalline metals (Wang et al.,

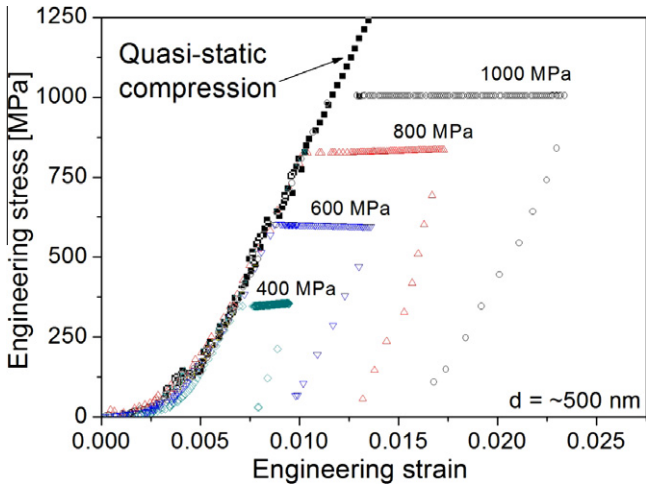

Fig. 3. Typical example of the change in engineering stress–strain curve with the applied stress (for the pillar sample having diameter of 500 nm). Normal quasi-static compression result is also shown.

2010); the creep curves consist of two regimes in the early stages: transient (primary) creep regime and steady-state (secondary) creep.

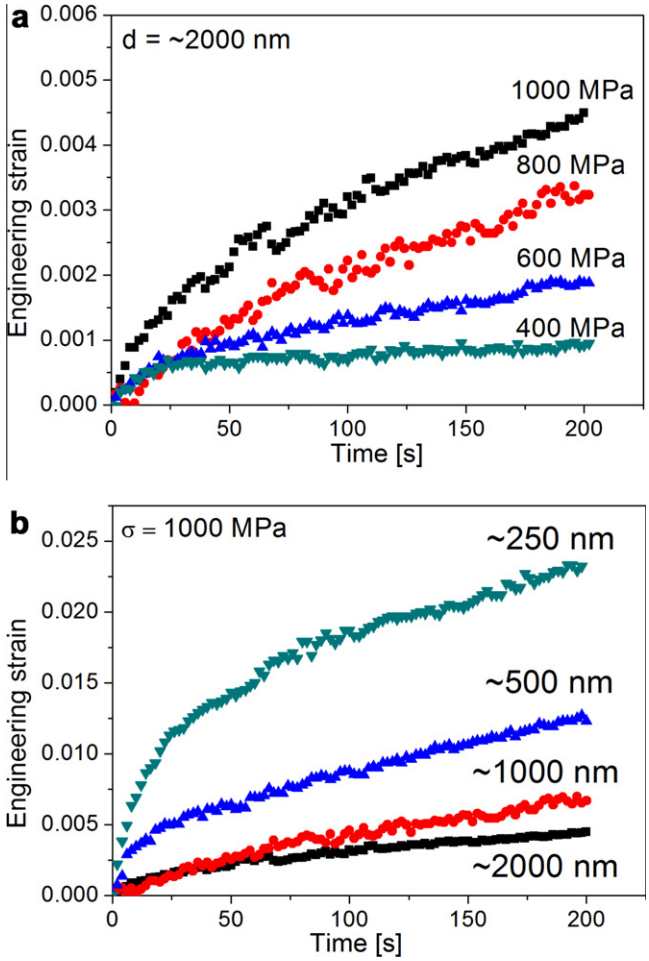

Fig. 4. Representative examples of creep strain–time curve: (a) effect of the applied stress; (b) effect of the pillar size.

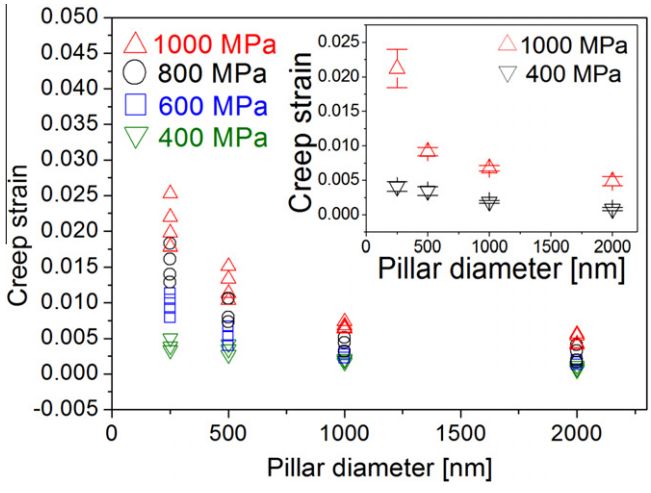

Fig. 5. Variation in creep strain as a function of pillar diameter. For clarifying the trend, 400 and 1000 MPa cases are separately shown in the inset figure.

The influences of d and σ on the creep amount are summarized in Fig. 5 where the total creep strain, ε_{total}, is plotted as a function of d. For clarity, the results obtained with the lowest and highest stress (400 and 1000 MPa, respectively) are separately shown in the inset of the figure. The following three points are noteworthy: First, for a given σ, ε_{total} increases with decreasing d. Second, for a given d, ε_{total} increases with increasing σ. Third, these two trends appear to be size- and stress-sensitive, i.e., they become more pronounced at smaller d and higher σ.

As mentioned before, some recent studies have reported the RT creep of metallic glasses using millimeter scale compression specimens. Thus, it is instructive to compare our data from micro- or nanometer scale specimens with those in the literature (Ke et al., 2011; Lee et al., 2008; Park et al., 2008; Park et al., 2009a,b) (see summary in Table 1). In comparison, the creep strains from micro-/nano-pillars (in Fig. 5) are order(s) of magnitude larger than those from millimeter samples (see Table 1). Note that such a direct comparison is fraught with some difficulties as the creep time in Table 1 is far longer than that in this work. The secondary creep regime (where the strain rate is the minimum) takes a substantially large portion of the observed creep response of the literature data. In contrast, primary creep regime (in which the strain rate is high) is dominant in the present pillar creep tests. Note also that the creep amount is markedly affected by structural state of the metallic glass (such as free volume amount and atomic packing density), and thus chemical composition and glass forming ability (Park et al., 2009a). These factors add additional complexities in direct comparison of the creep responses of different BMGs.

4. Discussion

4.1. Steady-state strain rate

One of the key parameters that is used to systematically analyze the time-dependent deformation behavior of a material is the creep strain rate, $\dot{\varepsilon}$. To estimate $\dot{\varepsilon}$, the creep curves (in Fig. 4) were fitted with the Garofalo's equation, which was originally suggested for analyzing conventional tensile creep (Garofalo, 1960):

$$\varepsilon = \varepsilon_0 + \alpha(1 - e^{-rt}) + \omega t \tag{1}$$

where ε_0 is an instantaneous strain during loading (which is 0 in Fig. 4), and α, ω, r are creep constants. In Fig. 6(a) the goodness of the fit of the experimental strain-time data with Eq. (1) is illustrated. High values of correlation coefficients ($R^2 > 0.97$) were obtained for all the creep curves. By differentiating Eq. (1) with respect to t, $\dot{\varepsilon}$ is obtained.

Fig. 6(b) shows the variation of $\dot{\varepsilon}$ as a function of t. At all the stress levels examined in this work, two distinct stages can be noted. In the first stage, $\dot{\varepsilon}$ decreases rapidly with t, which is akin to that seen in high temperature creep of crystalline materials, before reaching a constant plateau (second stage). In the creep of crystalline metals, the steady-state creep is often considered as a result of the balance between strain hardening (due to dislocation-mediated plastic flow and subsequent entanglement of the dislocations) and softening (recovery) (Dieter, 1988). In analogy, a steady-state condition of metallic glasses during homogeneous deformation may be regarded as a balance between free volume creation, which causes plastic flow softening, and its annihilation that results in hardening (Bhowmick et al., 2006; Yoo et al, 2009a). If this hypothesis is valid, a possible scenario that can be construed is that in the early stage, the applied stress induces the generation of excess free volume and thus mechanical softening (Argon, 1979; Schuh et al., 2007; Spaepen, 1977). Then, diffusive relaxation gradually comes into play and when it matches the rate of free volume production, steady state condition is attained. Although this type of transition to steady-state was previously observed during constant strain-rate tests at high temperatures of metallic glasses (near the glass transition temperature T_g) (Lu et al., 2010), it is noteworthy that such a transition is not expected to occur at RT. This is the first time that the influence of the applied stress on the steady-state strain rates at RT is reported. From Fig. 6(b), it is obvious that the estimated values of $\dot{\varepsilon}$ and the time for the transition from transient to steady-state creep regime, t_{trans}, are strongly dependent on σ with higher σ resulting in increased $\dot{\varepsilon}$ and t_{trans}. It is important to note that this is in contrast to that observed in crystalline metals where higher σ results in lower t_{trans}. This can be explained on the basis of the free volume theory that is widely used for phenomenological description of plastic deformation in metallic glasses (Spaepen, 1977). On one hand, the stress effect on the strain rate can be easily understood by Spaepen's general flow equation (Schuh et al., 2007; Spaepen, 1977) that can be easily converted to a relation between normal stress σ and steady-state strain rate $\dot{\varepsilon}_{ss}$:

Table 1
Summary of the room-temperature creep experiments on metallic glasses reported in literature.

Material	Sample diameter	Applied stress (% of σ_y)	Hold time	Creep strain (%)	Reference
$Cu_{65}Zr_{35}$	1 mm	1.98 GPa (90%)	12 h	0.40	(Lee et al., 2008; Park et al., 2008, 2009a,b)
		1.76 GPa (80%)		0.20	(Park et al., 2009a)
		1.54 GPa (70%)		0.13	(Park et al., 2009a)
		1.32 GPa (60%)		0.10	(Park et al., 2009a)
		1.10 GPa (50%)		0.07	(Park et al., 2009a)
$Cu_{57}Zr_{43}$	1 mm	1.80 GPa (90%)	12 h	0.25	(Park et al., 2008)
$Cu_{50}Zr_{50}$	1 mm	1.44 GPa (90%)	12 h	0.20	(Park et al., 2008)
$Zr_{46.75}Ti_{8.25}Cu_{7.5}Ni_{10}Be_{27.5}$	5 mm	1.46 GPa (80%)	5 h	0.0213	(Ke et al., 2011)

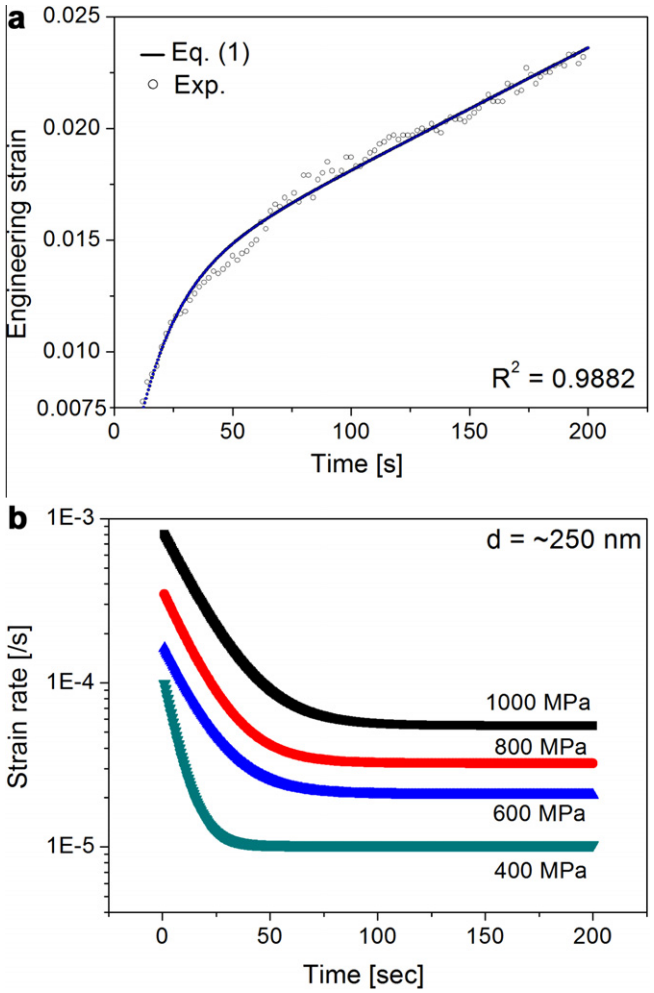

Fig. 6. Results of creep curve analysis; (a) experimental strain-time data and its fitting equation; (b) change in strain rate with holding time.

$$\dot{\varepsilon}_{ss} = A^* \exp\left(-\frac{\gamma \upsilon^*}{\upsilon_f}\right) \sinh\left(\frac{\sigma\Omega}{2\sqrt{3}kT}\right) \exp\left(-\frac{\Delta G^m}{kT}\right) \tag{2}$$

where A^* is the constant, γ is a geometrical factor that ranges between 0.5 and 1, υ^* is the atomic volume, υ_f is the average free volume per atom, k is the Boltzmann's constant, T is the absolute temperature, Ω is the atomic volume, G^m is the activation energy of motion. Accordingly, increasing σ would certainly result in an increase in $\dot{\varepsilon}_{ss}$.

If the steady-state condition is indeed a consequence of the balance between the free volume creation and annihilation, as proposed, the effect of σ on t_{trans} can be also rationalized on the basis of Spaepen's free volume theory (Spaepen, 1977). According to it, the amount of excess free volume that is created during the creep deformation is

$$\Delta^+ \upsilon_f = \frac{\gamma \upsilon^*}{\upsilon_f} \frac{2kT}{S} \left[\cosh\left(\frac{\sigma\Omega}{2\sqrt{3}kT}\right) - 1\right] N\nu \exp\left(-\frac{\Delta G^m}{kT}\right) \exp\left(-\frac{\gamma \upsilon^*}{\upsilon_f}\right) \tag{3}$$

where S is the elastic distortion energy, ν is the frequency, and N is the total number of the atoms. In Eq. (3), the process of free volume operation during creep can be regarded as a stress-assisted nucleation event. While Eq. (3) suggests that the amount of excess free volume increases with the applied shear stress τ (that can be estimated from the applied normal stress σ), the amount of the annihilation of free volume per jump can be expressed without stress term (Spaepen, 1977):

$$\Delta^- \upsilon_f = \frac{\upsilon^*}{n_D} N\nu \exp\left(-\frac{\gamma \upsilon^*}{\upsilon_f}\right) \exp\left(-\frac{\Delta G^m}{kT}\right) \tag{4}$$

where υ^*/n_D is amount of free volume annihilated per jump. This equation suggests that the diffusional annihilation can be affected by stress-induced structural state, and most importantly not by σ itself. Note that (i) the steady-state condition can

be achieved at $\Delta^{+}\upsilon_f = \Delta^{-}\upsilon_f$ and (ii) the creation amount $\Delta^{+}\upsilon_f$ is stress-dependent while the annihilation amount $\Delta^{-}\upsilon_f$ is not. Therefore it is reasonable to conclude that t_{trans} is directly affected by the level of σ.

4.2. Creep stress exponent

Fig. 7 shows the variation of $\dot{\varepsilon}_{ss}$ with σ for each pillar diameter. Data in this plot follows the well known power-law:

$$\dot{\varepsilon} = K\sigma^{n}, \tag{5}$$

where K is the material- and temperature-dependent factor and n $\left(=\frac{\partial \ln \dot{\varepsilon}}{\partial \ln \sigma}\right)$ is the creep stress exponent. The value of n that was determined from Fig. 7 is plotted in Fig. 8 as a function of d. It clearly indicates that the creep behavior of metallic glasses is size-dependent; as the pillar diameter decreases, the value of n increases. The power law fits in Fig. 7 are extrapolated to the global quasi-static σ_y to estimate the strain rate at σ_y, which increases rapidly with reducing d, i.e., $\dot{\varepsilon} \sim 9.8 \times 10^{-5}$, 1.7×10^{-4}, 2.9×10^{-4}, and 1×10^{-3}/s for $d = \sim$2000, 1000, 500, 250 nm, respectively.

The power-law fitting led to the values of n as 2.54, 2.64, 2.97, and 3.21 for $d = \sim$2000, 1000, 500, and 250 nm, respectively. From the viewpoint of the classical creep mechanisms developed for crystalline metals and alloys, these n values are between diffusion-dominant creep (n = 1–2) and dislocation-dominant creep (n = 3–8). Recent work reported that elastostatic stress can induce a small amount of structural disorder whose size may be much smaller than so-called shear transformation zones (STZs) (Albano and Falk, 2005; Falk and Langer, 1998; Ke et al., 2011; Park et al., 2008; Yoo et al., 2010a). If this scenario holds valid, it is possible that the homogeneous deformation observed in this work is mainly controlled by atomic diffusion in a similar fashion. This provides an interesting way to understand the size effect on the creep behavior.

A comparison of the data obtained in the present work to that reported in literature (mostly in the form of strain-rate sensitivity m (=1/n)) brings out the following two points. First, our data fall within the range of n values reported for non-Newtonian homogeneous deformation, which are obtained from either constant strain-rate tests (Johnson et al., 2002; Kawamura et al., 1998; Nieh et al., 2001) or constant load tests (Csach et al., 1998; Heggen et al., 2005) at temperatures near T_g; e.g., n = 1.4–3.7 (Kawamura et al., 1998), ~2 (Csach et al., 1998; Heggen et al., 2005; Nieh et al., 2001), 2–6 (Johnson et al., 2002). In contrast, only one paper has reported the relation between creep stress and strain rate at RT: the n value estimate from the work on $Cu_{65}Zr_{35}$ (Park et al., 2009a) is ~1.23. Since the diameter of the compressive samples used in that work is 1 mm, the higher n values observed in the present work are possibly be due to the enhanced creep in the smaller diameter samples used.

It is possible to qualitatively estimate the pillar size effect on the relative amount of free volume creation by making a key assumption that the homogeneous creep deformation at RT can induce structural changes leading to anisotropic structure (Harmon et al., 2007; Ke et al., 2011). At low σ and high temperatures ($\sigma\Omega << kT$), the term $sinh(\sigma\Omega/2\sqrt{3}kT)$ in Eq. (2) can be reduced to $\sigma\Omega/2\sqrt{3}kT$. In this case, the creep stress exponent n in Eq. (5) is unity, implying the deformation is Newtonian (Schuh et al., 2007). At sufficiently higher stress level ($\sigma\Omega >> kT$), $\Delta^{+}\upsilon_f$ is very large, but $\Delta^{-}\upsilon_f$ is somewhat negligible. Therefore, Eq. (2) can be rearranged as (Schuh et al., 2007)

$$\dot{\varepsilon} = B^{*} \exp\left(-\frac{\gamma \upsilon^{*}}{\upsilon_f}\right) \exp\left(-\frac{\Delta G^{m} - \sigma\Omega}{kT}\right). \tag{6}$$

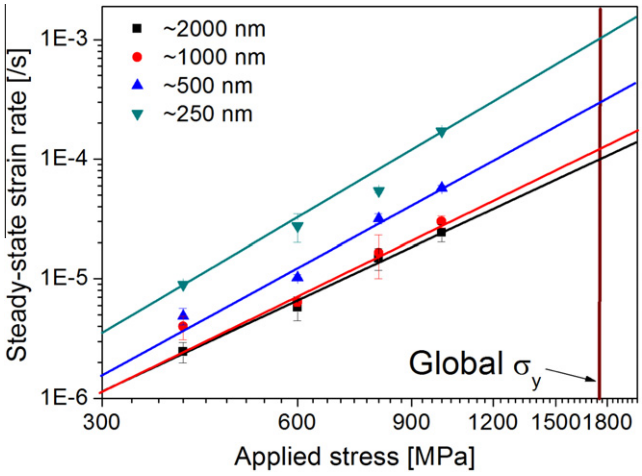

Fig. 7. Variation in the steady-state strain rate with the applied stress. The correlation factor R^2 is 0.96, 0.95, 0.94, and 0.96 for $d = \sim$250, ~500, ~1000, and ~2000, respectively.

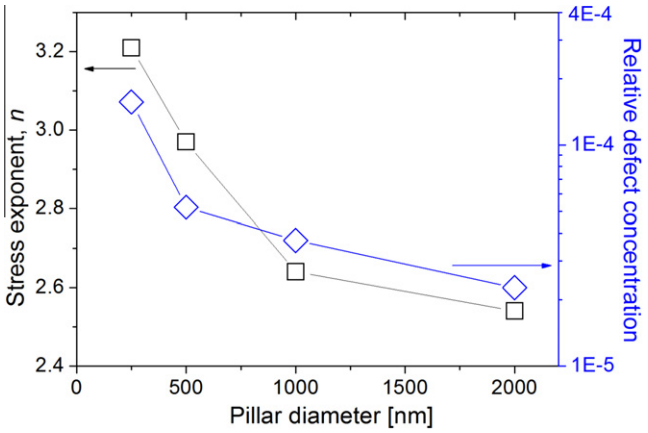

Fig. 8. Influence of pillar size on the stress exponent n (obtained from the slope of linear relations shown in Fig. 6) and (b) the relative amount of free volume creation.

where B^* is a constant. In this case, $n \neq 1$, and can increase to extremely high value (i.e., for non-Newtonian unstable flow) as σ and strain rate are increased. The transition from Newtonian to non-Newtonian flow depends on the testing temperature (Csach et al., 1998; Heggen et al., 2005; Johnson et al., 2002; Kawamura et al., 1998; Lu et al., 2010; Nieh et al., 2001). From Eqs. (2) and (5), the relation between σ and $\dot{\varepsilon}$ can be rewritten as:

$$\frac{\dot{\varepsilon}}{\sigma^n} = C^* exp\left(-\frac{\gamma \upsilon^*}{\upsilon_f}\right). \tag{7}$$

where C^* is a constant.

When an external stress is applied, excess free volume is created by the diffusive atomic jumps (Cohen and Turnbull, 1959; Spaepen, 1977; Turnbull and Cohen, 1961, 1970). The term $\exp(-\gamma\upsilon^*/\upsilon_f)$ (that is the potential jump site or the defect concentration) is an indicator for the amount of free volume created. To estimate the influence of pillar size on the defect concentration clearly, one may use the extrapolated steady-state strain rates at a certain high stress value (e.g., the global σ_y as in this work) because the fluctuation in experimental data can often mislead the trend of size effect. Thus, from Eq. (7), the relative defect concentration is estimated as a function of d, which is additionally plotted in Fig. 8. It is evident that, with reducing d, the defect concentration increases. For example, the relative defect concentration (that is the normalized difference in the left-hand term of Eq. (7) between two pillars with different d) in the pillar with $d = \sim$250 nm is approximately six times higher than that in $d = \sim$2000 nm.

A pertinent question that arises at this juncture is what is the physical phenomenon that leads to the enhanced creep in smaller pillars? A clue for the answer can be gained from the fact that free surfaces of the creep specimens provide an efficient diffusion path vis-à-vis the bulk. This is particularly prominent at the nano-scale, where the activation energy for diffusion is significantly lowered as the surface-to-volume ratio (SVR) increases (Guisbiers and Buchaillot, 2008). Thus, the SVR is an important parameter to consider for understanding the marked increase in the ε and $\dot{\varepsilon}$ with reducing d. In this regard, it should be noted that the volume diffusion in metallic glasses is far faster than that in crystalline metals, because there is no long range order in the atomic arrangement of the glasses and hence volume diffusion in them is more similar to the diffusion along grain boundaries (having an amorphous-like structure) in polycrystalline aggregates. Although the diffusivity of the so-called 'short circuit diffusion' along surface or grain boundaries in a crystalline metal may vary depending on the crystallographic orientation, it is often roughly approximated by summarizing the data in a random direction (Gjostein, 1973; Gleiter and Chalmer, 1972; Nishizawa, 2008); for a surface diffusion,

$$D_{surf} \approx 7 \times 10^{-6} exp\left(-\frac{9.3 \times 10^{-23} T_m}{kT}\right) (\text{in m}^2/\text{s}) \tag{8}$$

and for a grain boundary diffusion

$$D_{GB} \approx 4 \times 10^{-5} exp\left(-\frac{1.36 \times 10^{-22} T_m}{kT}\right) (\text{in m}^2/\text{s}) \tag{9}$$

where T_m is the melting temperature. Note again that Eqs. (8) and (9) are conceivably applied to any crystalline material independent of crystal structure. For adapting these to the metallic glasses, the glass transition temperature, T_g, may be more appropriate parameter than T_m. By putting T_g of 673 K for the examined BMG (Yoo et al., 2009b) and testing temperature T of 298 K into the above equations, we could estimate $D_{surf} \approx 1.72 \times 10^{-12}$ m^2/s and $D_{GB} \approx 8.63 \times 10^{-15}$ m^2/s and thus the ratio of D_{surf}/D_{GB} is about 200. This large ratio suggests that SVR can significantly affect the time-dependent deformation charac-

teristics of the amorphous pillars. By assuming a perfect cylindrical geometry for the pillars, the SVRs are calculated as 1.8×10^{-4}, 3.6×10^{-4}, 7.2×10^{-4}, and 1.4×10^{-3}/nm for $d = \sim$2000, 1000, 500, and 250 nm, respectively. This rapid increase in the ratio with reducing size provides a clue for understanding not only the largely enhanced ε and $\dot{\varepsilon}$ in smaller pillars but also their higher amount of free volume created by atomic diffusive jumps.

5. Conclusion

In the present work, uniaxial compression creep tests were performed on micro-/nano-sized pillars of a Zr-based BMG to investigate the influence of sample size on the room-temperature creep behavior of metallic glass. The primary results of this investigation are:

- The load-displacement data and the postmortem SEM analysis suggested that, in all examined pillars, the creep deformation indeed occurred at RT is homogeneous in nature.
- The amount of time-dependent plastic strain is significantly affected by both the applied stress and the pillar size; i.e. with increasing stress or decreasing pillar diameter, the total strain was largely increased.
- Experimental data showed that the creep test certainly reached at the steady-state condition that may be regarded as a balance between free volume creation (softening) and annihilation (hardening). The applied stress was found to straightforwardly affect not only the steady-state strain rate value but also the critical holding time required for the primary-to-secondary-regime transition, which could be analyzed through free volume theory.
- There was a linear relationship between $\log(\dot{\varepsilon})$ vs. $\log(\sigma)$, and the creep stress exponent n (estimated from the slope of the plot) was not unity and increased from $\sim$2.5 to $\sim$3.2 with reducing pillar size.
- The largely increased time-dependent room temperature plasticity of the metallic glass nano-/micro-pillars and its size effect are discussed in terms of the increases in both relative defect concentration and surface-to-volume ratio with decreasing pillar size.

Acknowledgement

This research was supported by Basic Science Research Program through the National Research Foundation of Korea (NRF) funded by the Ministry of Education, Science and Technology (No. 2010-0025526). The work at ORNL (H.B.) was supported by the US Department of Energy, Office of Basic Energy Sciences, Materials Sciences and Engineering Division.

References

Albano, F., Falk, M.L., 2005. Shear softening and structure in a simulated three-dimensional binary glass. J. Chem. Phys. 122, 154508.
Argon, A.S., 1979. Plastic deformation in metallic glasses. Acta Metall. 27, 47–58.
Bei, H., Lu, Z.P., Shim, S., Chen, G., George, E.P., 2010. Specimen size effects on Zr-based bulk metallic glasses investigated by uniaxial compression and spherical nanoindentation. Metall. Mater. Trans. A 41, 1735–1742.
Bhowmick, R., Raghavan, R., Chattopadhyay, K., Ramamurty, U., 2006. Plastic flow softening in a bulk metallic glass. Acta Mater. 54, 4221–4228.
Castellero, A., Moser, B., Uhlenhaut, D.I., Dalla Torre, F.H., Löffler, J.F., 2008. Room-temperature creep and structural relaxation of Mg–Cu–Y metallic glasses. Acta Mater. 56, 3777–3785.
Chen, C.Q., Pei, Y.T., De Hosson, J.T.M., 2010. Effects of size on the mechanical response of metallic glasses investigated through in situ TEM bending and compression experiments. Acta Mater. 58, 189–200.
Chen, M., 2011. A brief overview of bulk metallic glasses. NPG Asia Mater. 3, 82–90.
Cohen, M.H., Turnbull, D., 1959. Molecular transport in liquids and glasses. J. Chem. Phys. 31, 1164–1169.
Csach, K., Fursova, Y.V., Khonik, V.A., Ocelik, V., 1998. Non-Newtonian plastic flow of a Ni–Si–B metallic glass at low stresses. Scripta Mater. 39, 1377–1382.
Dieter, G.E., 1988. Mechanical Metallurgy. McGraw-Hill, London.
Dubach, A., Raghavan, R., Löffler, J.F., Michler, J., Ramamurty, U., 2009. Micropillar compression studies on a bulk metallic glass in different structural states. Scripta Mater. 60, 567–570.
Falk, M.L., Langer, J.S., 1998. Dynamics of viscoplastic deformation in amorphous solids. Phys. Rev. E 57, 7192–7205.
Garofalo, F., 1960. ASTM Spec. Tech. Publ. 283, 82–98.
Gjostein, N.A., 1973. ASM Seminar on Diffusion. ASM International, Metals Park, OH.
Gleiter, H., Chalmer, B., 1972. Grain-boundary diffusion. Prog. Mater. Sci. 16, 77–112.
Greer, J.R., De Hosson, J.T.M., 2011. Plasticity in small-sized metallic systems: intrinsic versus extrinsic size effect. Prog. Mater. Sci. 56, 654–724.
Guisbiers, G., Buchaillot, L., 2008. Size and shape effects on creep and diffusion at the nanoscale. Nanotechnology 19, 435701.
Harmon, J.S., Demetriou, M.D., Johnson, W.L., Samwer, K., 2007. An elastic to plastic transition in metallic glass-forming liquids. Phys. Rev. Lett. 99, 135502.
Heggen, M., Spaepen, F., Feuerbacher, M., 2005. Creation and annihilation of free volume during homogeneous flow of a metallic glass. J. Appl. Phys. 97, 033506.
Huang, Y.J., Shen, J., Sun, J.F., 2007. Bulk metallic glasses: smaller is softer. Appl. Phys. Lett. 90, 081919.
Huang, Y.J., Chiu, Y.L., Shen, J., Chen, J.J.J., Sun, J.F., 2009a. Indentation creep of a Ti-based metallic glass. J. Mater. Res. 24, 993–997.
Huang, Y.J., Shen, J., Chiu, Y.L., Chen, J.J.J., Sun, J.F., 2009b. Indentation creep of an Fe-based bulk metallic glass. Intermetallics 17, 190–194.
Inoue, A., Takeuchi, A., 2011. Recent development and application products of bulk glassy alloys. Acta Mater. 59, 2243–2267.
Jang, D., Greer, J.R., 2010. Transition from a strong-yet-brittle to a stronger-and-ductile state by size reduction of metallic glasses. Nature Mater. 9, 215–219.
Jang, D., Gross, C.T., Greer, J.R., 2011a. Effects of size on the strength and deformation mechanism in Zr-based metallic glasses. Int. J. Plasticity 27, 858–867.
Jang, J.-I., Yoo, B.-G., Kim, Y.-J., Choi, I.-C., Bei, H., 2011b. Indentation size effect in bulk metallic glass. Scripta Mater. 64, 753–756.
Johnson, W.L., Lu, J., Demetriou, M.D., 2002. Deformation and flow in bulk metallic glasses and deeply undercooled glass forming liquids—a self consistent dynamic free volume model. Intermetallics 10, 1039–1046.
Kawamura, Y., Nakamura, T., Inoue, A., 1998. Superplasticity in Pd40Ni40P20 metallic glass. Scripta Mater. 39, 301–306.

Ke, H.B., Wen, P., Peng, H.L., Wang, W.H., Greer, A.L., 2011. Homogeneous deformation of metallic glass at room temperature reveals large dilatation. Scripta Mater. 2011 (64), 966–969.
Kim, J.-Y., Greer, J.R., 2009. Tensile and compressive behavior of gold and molybdenum single crystals at the nano-scale. Acta Mater. 57, 5245–5253.
Kim, Y.-J., Son, K., Choi, I.-C., Choi, I.-S., Park, W.I., Jang, J.-I., 2011. Exploring nanomechanical behavior of silicon nanowires: AFM bending versus nanoindentation. Adv. Func. Mater. 2011 (21), 279–286.
Kumar, G., Desai, A., Schroers, J., 2011. Bulk metallic glass: the smaller the better. Adv. Mater. 2011 (23), 461.
Lee, S.-J., Yoo, B.-G., Jang, J.-I., Lee, J.-C., 2008. Irreversible structural change of an amorphous alloy induced by elastostatic stress and its influence on the mechanical properties. Met. Mater. Int. 14, 9–13.
Li, W.H., Shin, K., Lee, C.G., Wei, B.C., Zhang, T.H., He, Y.Z., 2008. The characterization of creep and time-dependent properties of bulk metallic glasses using nanoindentation. Mater. Sci. Eng. A 2008 (478), 371–375.
Lu, J., Ravichandran, G., Johnson, W.L., 2010. Deformation behavior of the $Zr_{41.2}Ti_{13.8}Cu_{12.5}Ni_{10}Be_{22.5}$ bulk metallic glass over a wide range of strain-rates and temperatures. Acta Mater. 51, 3429–3443.
Nieh, T.G., Wadsworth, J., Liu, C.T., Ohkubo, T., Hirotsu, Y., 2001. Plasticity and structural instability in a bulk metallic glass deformed in the supercooled liquid region. Acta Mater. 49, 2887–2896.
Nishizawa, T., 2008. Thermodynamics of Microstructures. ASM International, Materials Park, OH.
Park, K.-W., Lee, C.-M., Wakeda, M., Shibutani, Y., Falk, M.L., Lee, J.-C., 2008. Elastostatically induced structural disordering in amorphous alloys. Acta Mater. 56, 5440–5450.
Park, K.-W., Lee, C.-M., Kim, H.-J., Lee, J.-H., Lee, J.-C., 2009a. A methodology of enhancing the plasticity of amorphous alloys: elastostatic compression at room temperature. Mater. Sci. Eng. A 499, 529–533.
Park, K.-W., Lee, C.-M., Lee, J.-C., 2009b. Plasticity of amorphous alloys: 1. Homogeneous deformation. J. Korean Inst. Met. Mater. 47, 759–772.
Schroers, J., 2010. Processing of bulk metallic glass. Adv. Mater. 22, 1566–1597.
Schuh, C.A., Hufnagel, T.C., Ramamurty, U., 2007. Mechanical behavior of amorphous alloys. Acta Mater. 55, 4067–4109.
Schuster, B.E., Wei, Q., Hufnagel, T.C., Ramesh, K.T., 2008. Size-independent strength and deformation mode in compression of a Pd-based metallic glass. Acta Mater. 56, 5091–5100.
Shan, Z.W., Li, J., Cheng, Y.Q., Minor, A.M., Syed Asif, S.A., Warren, O.L., Ma, E., 2008. Plastic flow and failure resistance of metallic glass: insight from in situ compression of nanopillars. Phy. Rev. B 77, 155419.
Spaepen, F., 1977. A microscopic mechanism for steady state inhomogeneous flow in metallic glasses. Acta Metall. 25, 407–415.
Turnbull, D., Cohen, M.H., 1961. Free-volume model of the amorphous phase: glass transition. J. Chem. Phys. 34, 120–125.
Turnbull, D., Cohen, M.H., 1970. On the free-volume model of the liquid-glass transition. J. Chem. Phys. 52, 3038–3041.
Van Steenberge, N., Sort, J., Concustell, A., Das, J., Scudino, S., Surinach, S., Eckert, J., Baro, M.D., 2007. Dynamic softening and indentation size effect in a Zr-based bulk glass-forming alloy. Scripta Mater. 56, 605–608.
Volkert, C.A., Donohue, A., Spaepen, F., 2008. Effect of sample size on deformation in amorphous metals. J. Appl. Phys. 103, 083539.
Wang, C.L., Lai, Y.H., Huang, J.C., Nieh, T.G., 2010. Creep of nanocrystalline nickel: a direct comparison between uniaxial and nanoindentation creep. Scripta Mater. 2010 (62), 175–178.
Wang, W.H., 2009. Bulk metallic glasses with functional physical properties. Adv. Mater. 21, 4524–4544.
Ye, J.C., Lu, J., Yang, Y., Liaw, P.K., 2009. Study of the intrinsic ductile to brittle transition mechanism of metallic glasses. Acta Mater. 2009 (57), 6037–6046.
Yoo, B.-G., Kim, Y.-J., Oh, J.-H., Ramamurty, U., Jang, J.-I., 2009a. On the hardness of shear bands in amorphous alloys. Scripta Mater. 61, 951–954.
Yoo, B.-G., Park, K.-W., Lee, J.-C., Ramamurty, U., Jang, J.-I., 2009b. Role of free volume in strain softening of as-cast and annealed bulk metallic glass. J. Mater. Res. 24, 1405–1416.
Yoo, B.-G., Kim, K.-S., Oh, J.-H., Ramamurty, U., Jang, J.-I., 2010a. Room temperature creep in amorphous alloys: influence of initial strain and free volume. Scripta Mater. 63, 1205–1208.
Yoo, B.-G., Oh, J.-H., Kim, Y.-J., Park, K.-W., Lee, J.-C., Jang, J.-I., 2010b. Nanoindentation analysis of time-dependent deformation in as-cast and annealed Cu–Zr bulk metallic glass. Intermetallics 18, 1898–1901.
Zhang, H., Schuster, B.E., Wei, Q., Ramesh, K.T., 2006. The design of accurate micro-compression experiments. Scripta Mater. 54, 181–186.